Measurement Science and Technology

PAPER

Indoor altitude estimation assisted by inertial compensation and online floor modeling

To cite this article: Ming Xia *et al* 2024 *Meas. Sci. Technol.* **35** 126302

IOP Publishing Measurement Science and Technology
Meas. Sci. Technol. **35** (2024) 126302 (11pp) https://doi.org/10.1088/1361-6501/ad7487

Indoor altitude estimation assisted by inertial compensation and online floor modeling

Ming Xia[1], Jiale Wang[1,*], Chuang Shi[1] and Weisong Wen[2]

[1] School of Electronic and Information Engineering, Beihang University, Beijing 100191, People's Republic of China
[2] Department of Aeronautical and Aviation Engineering, The Hong Kong Polytechnic University, Hung Hom, Kowloon, Hong Kong Special Administrative Region of China, People's Republic of China

E-mail: by1902036@buaa.edu.cn

Received 6 May 2024, revised 18 August 2024
Accepted for publication 28 August 2024
Published 5 September 2024

Abstract

Indoor pedestrian altitude information plays a key role in such applications as emergency relief and military reconnaissance. However, height errors of inertial positioning grow without boundary because of the altitude channel divergence of the Strap-down Inertial Navigation System. This article proposes a new vertical location method based on the foot-mounted Inertial Measurement Unit and online floor modeling. First, the number of stairs at each step is calculated after the height of each step is corrected by the error compensation model. Second, the prior height is estimated by utilizing the number of stairs and the stair height. Then, the key point library related to the floor is built online. Finally, the error correction of the vertical displacement is carried out by matching the prior height with the key point library. The gait classification shows that the accuracy based on the error compensation model can reach up to 99%. Moreover, the maximum altitude error is less than 1 m and the accumulated vertical positioning errors are eliminated completely when a pedestrian walks up and down inside a multi-story building, and all these have verified accuracy and robustness of vertical indoor positioning.

Keywords: altitude estimation, inertial compensation, floor modeling, gait classification, indoor positioning

1. Introduction

Vertical location has generated a high level of research interest and become an essential topic in the field of Indoor Pedestrian Navigation (IPN) owing to an increasing number of large buildings with complex structures [1]. Compared with horizontal errors, vertical positioning accuracy is more critical for IPN, because an altitude error of just a few meters can lead to incorrect floor identification.

Multiple types of techniques have been employed to implement vertical trajectory determination. The traditional technique, Global Navigation Satellite Systems (GNSS), requires a clear sky view, and is thus ineffective when satellite signals are totally blocked or severely attenuated indoors [2, 3]. One alternative is wireless communication positioning, such as Wireless Fidelity (WIFI) [4, 5], Ultra Wideband (UWB) [6], Bluetooth [7], and cellular network [8–10]. They all rely on existing equipment or require new deployments. For instance, WIFI needs a wide range of beacon nodes and cellular network relies on base stations.

Another alternative to GNSS is sensor-based technique, which does not need external facilities. In [11], vertical location is obtained by barometer based on the principle that air pressure decreases with altitude. In [12], Zhang *et al* install a barometer on every floor to form a correspondence table

* Author to whom any correspondence should be addressed.

between air pressure and floor as reference. Although the method based on barometric pressure can provide an accurate floor level, they are sensitive to local pressure conditions. A solution to this problem is self-contained navigation based on inertial measurement unit (IMU), which is strongly independent and less affected by the environment [13]. Due to the development of Micro-Electro-Mechanical System (MEMS) technology, MEMS-IMU has received much attention due to its advantages of compactness, light weight, and low power, which meet the needs of pedestrians' vertical positioning.

MEMS -IMU is usually fixed on foot or trunk for height measurement. One way to install an inertial unit on the user's trunk employs the pedestrian dead reckoning (PDR) algorithm, which is only used for horizontal position estimation [14]. Another widely used IMU-based scheme, based on the Strap-down Inertial Navigation System (SINS) algorithm, straps IMU on a user's foot and calculates the user position by integrating sensor output [15, 16]. The altitude is obtained by double integrating the acceleration in SINS algorithm [17]. As inherent sensor errors cause the coupling of gravity and motion acceleration in the vertical direction, SINS-based altitude estimation suffers from the divergence problem. Usually, the Zero Velocity Update (ZUPT) method is applied to improve the positioning performance of SINS-based IPN system [18]. When the velocity error obtained from ZUPT is fed back to an estimation filter such as Extended Kalman Filter (EKF), position and attitude errors would be restricted [19].

Nevertheless, vertical positioning errors are still difficult to constrain in wearable inertial system, because the ZUPT method cannot eliminate the effect of gravity residuals on motion acceleration [20]. Ideally, positioning errors in a vertical direction can be bounded by fusing SINS-based height estimate and height observations from a barometer [21, 22], but barometers are susceptible to environmental factors including air flow, temperature variations, air conditioning systems, etc. For this reason, height error information from external facilities, such as radio frequency identification, WIFI, and UWB, is obtained as the measurement of EKF, resulting in integrated multi-sensor IPN system [6, 23–25]. Unfortunately, the signal interference of different floors will cause inaccurate estimation because there are many wireless access points distributed in a crowded indoor environment and the signals cannot be completely obstructed by walls. To address this problem, Qiu *et al* [26] propose a Denavit-Hartenberg (DH) method, utilizing three inertial sensors and the relative motion of body joints to suppress drift. However, this method is limited by power supply, weight and synchronization. In addition, Puyol *et al* in [27] introduce the autoregressive integrated moving average (ARIMA) to model vertical displacement errors in IMU-based IPN system; however, this approach is limited by high computational complexity.

The vertical displacement of pedestrians in buildings is determined by the stair height and step number in IMU-based IPN system [14]. Given that the height of each step in and around the same building is fixed, the altitude is mainly determined by the stair number of stairs crossed in each step cycle, which is related with gait recognition [28]. Inspired by this idea, Abdulrahim *et al* [29] set altitude thresholds for different steps during a pedestrian's walking, and the pedestrian's motion state (upstairs, downstairs, and horizontal movements) can be identified by comparing the height change value of adjacent zero velocity points with the altitude threshold. A major drawback of the fixed threshold is that it cannot be adjusted adaptively according to the characteristics of pedestrian motion. Diaz *et al* [30] propose the height update (HUPT) algorithm that exploits the pitch of the shoe-mounted sensor to seamlessly recognize whether the user is walking horizontally or climbing stairs. Although this method does not require empirical thresholds, it only adapts to standard walking. In addition, the machine learning techniques are applied to assess and improve gait recognition accuracy [31]. Wagstaff *et al* [32] train a support vector machine (SVM) classifier using inertial data recorded by a single foot-mounted sensor to differentiate motion types, but the classification results may be ineffective when the level of noise is high. In [33], artificial neural network (ANN) is used to predict motion types using the data acquired from gyroscopes and accelerometers placed on foot. Nevertheless, ANN has difficulty in interpretability, and requires a large amount of data to perform better than other techniques. The bidirectional long short-term memory recurrent neural network (BLSTM-RNN) [34] is proposed as a gait classifier based on a single IMU, but requires expensive GPUs and multiple devices to train complex models. Although a variety of other classifiers have been used in previous work, such as naive Bayes [35], decision trees [36], k-nearest neighbor (KNN) [37], and random forests (RF) [38], their improvement in overall accuracy is still limited.

In summary, many existing infrastructure-based, barometric or gait recognition-aided IPN systems have achieved relatively high precision of vertical positioning accuracy for normal walking. However, if the locations of wireless access points (APs) change, air pressure fluctuates, or human motion is complicated, it remains a challenge to complete altitude estimation. In this paper, we propose a height estimation method, using IMU-based IPN system and online floor modeling. Specifically, the height variation of each step is calculated according to INS mechanism and corrected by error compensation model. Then, a gait classifier based on height variation is constructure to estimate the priori height at each step, and the key point library related to the floor is built or updated. Finally, further height calibration is carried out by matching the key point library with the priori height.

The rest of this paper consists of six sections. Section 2 expounds INS mechanization and section 3 introduces the estimation of prior height, involving gait phase identification, height error compensation model building, gait recognition, and estimation of a prior height. In section 4 the height calibration with the library of floor key points is presented, including the development for the library and floor matching. Experiments and analysis are provided in section 5, and the conclusion is given in section 6.

2. INS mechanization in IPN

The accelerometer contained in an IMU will output motion accelerations when an external force is imposed. According to Newton's law of motion, by integrating the motion acceleration, the velocity and position can be estimated when the initial attitude, velocity and position are known. Similarly, the gyroscope in the IMU can sense the rotation of the attached carrier. The attitude can be calculated by the integral of gyroscopic measurements [6].

In figure 1, we show the architecture diagram of the altitude estimation algorithm based on foot-mounted IMU. In this paper, two main coordinate frames play an important role: the body frame $\{b\}$, formed by the axes of MEMS-IMU, and the navigation frame $\{n\}$, locally defined with axes consistent with the east, north, and up directions (ENU). These two frames are demoted with the superscripts b and n, respectively. This system only includes MEMS-IMU, which provides the 3-axis accelerometer, 3-axis gyroscope, and 3-axis magnetometer readings, represented by $[f_x,f_y,f_z]$, $[\omega_x,\omega_y,\omega_z]$, and $[\mathrm{mag}_x,\mathrm{mag}_y,\mathrm{mag}_z]$ in the body frame, respectively. Magnetometer is only utilized for IMU initialization.

More complicated computations are necessary in IMU-based IPN system. Once measured in b-frame, the acceleration is needed to be converted to n-frame to estimate motion parameters. However, the transformation of the coordinate system is affected by earth rotation and curvature. To remove these effects, SINS algorithm has to be implemented in navigation coordinate system [39]. First, the rotation matrix is applied to transform the accelerometer measurement from b-frame to n-frame. As for the latter, since the low-cost inertial sensors are insensitive to the rotation of the earth, calculations related to this rotation are all ignored in SINS algorithm [40].

Navigation parameters (attitude, velocity and position) are solved by the following differential equations:

$$\begin{cases} \dot{C}_b^n = C_b^n \Omega^b \\ \dot{V}^n = C_b^n f^b + g^n \\ \dot{P}^n = V^n \end{cases} \tag{1}$$

where, C_b^n represents the rotation matrix to rotate a vector from b-frame to the n-frame; V^n and P^n refer to the velocity vector and displacement respectively; g^n denotes the local gravity vector; f^b represents the accelerometer measurement vector; Ω^b is the skew symmetric matrix of angular rates, defined as:

$$\Omega^b = \begin{bmatrix} 0 & -\omega_z & \omega_y \\ \omega_z & 0 & -\omega_x \\ -\omega_y & \omega_x & 0 \end{bmatrix} \tag{2}$$

where, ω_x, ω_y, and ω_z are gyroscopic measurements from the x-axis, y-axis, and z-axis in b-frame, respectively.

The vertical acceleration in n-frame comprises gravity components and the gravitational acceleration cannot be fully removed, which leads to the height channel divergence of SINS. If pedestrian's altitude is obtained by the double integral of the vertical acceleration in IMU-based IPN system, height errors will grow without boundary. Thereupon, it is necessary to limit the height error growth.

3. Estimation of prior height

The walking gait of humans has a periodic nature. The gait cycle consists of two phases: the stance phase and stride phase. Since the height is constant during the stance phase, the height changes occur mainly during the stride phase. In addition, the height change at each step is related with the gait state including horizontal, downstairs, and upstairs movements. Thereupon, constraining vertical drift in single IMU-based SINS solution by exploiting gait motion is our aim.

3.1. Gait phase detection

The two phases, stance phase and moving stride phase, are repeated periodically and rapidly, each of which lasts about 0.1∼0.3 s. During the stance phase, velocity-dependent errors are applied as pseudo-measurements to EKF, which utilizes these measurements as correct knowledge and estimates the errors in position, velocity and attitude. In addition, features extracted during the stride phase play a key role in gait recognition in each step cycle, so it is necessary to detect and distinguish the two phases. To detect the gait phase during walk, one can use a shoe-embedded high resolution pressure sensor which perceives the pressure exerted by foot touching the ground during the stance phase [41]. However, the main objective of this paper is to exploit single IMU sensor, so we will only utilize IMU data for stance or swing detection.

The stance phase of a step is usually detected based on the total acceleration (i.e. the norm of acceleration components) and total angular rate. Meanwhile, to increase the robustness of detection, the sample variance of the total acceleration and total angular rate within an appropriate time window is also used [18]. In our IPN method, a criterion called the generalized likelihood ratio test (GLRT) is used for stance detection. GLRT converts stance detection to binary hypothesis testing, and its output can be expressed as:

$$T_k(a,\omega) = \frac{1}{W}\sum_{l\in L_k}\left(\frac{\|\omega_l\|^2}{\sigma_\omega^2} + \frac{1}{\sigma_{\mathrm{acc}}^2}\left\|a_l - \frac{g^*\overline{\mathrm{acc}}_k}{\|\overline{\mathrm{acc}}_k\|}\right\|^2\right) \tag{3}$$

where, L_k is a sliding window with length W centered around k, a_l, $\omega_l \in \mathbb{R}^{1\times 3}$ represent inertial measurements at l-sampling time, σ_{acc}^2 and σ_ω^2 are the variances of acceleration and angular rate measurements respectively, $\|\cdot\|$ represents 2-norm, $\overline{\mathrm{acc}}_k$ denotes the average value of acceleration in the sliding window, and g is the local gravitational acceleration.

Then the condition for stance detection is stated as:

$$PH_{\mathrm{stance},k} = \begin{cases} 1, & T_k(a,\omega) < \gamma_{\mathrm{GLRT}} \\ 0, & \text{others} \end{cases} \tag{4}$$

where, γ_{GLRT} is GLRT threshold. We can interpret the expressions (3) and (4) as follows: when the mean square error of fitting a vector of magnitude g with the direction of the average specific force vector to the accelerometer data in combination

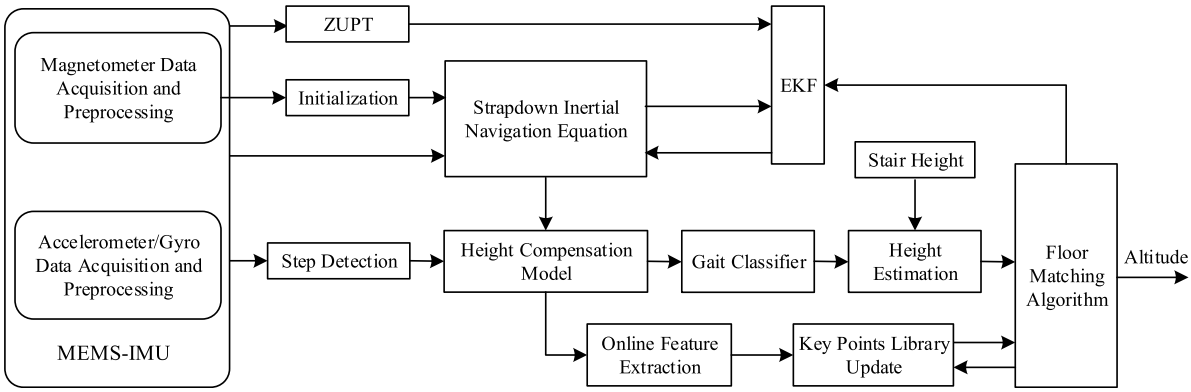

Figure 1. Architecture diagram of pedestrian's vertical positioning system based on foot-mounted IMU.

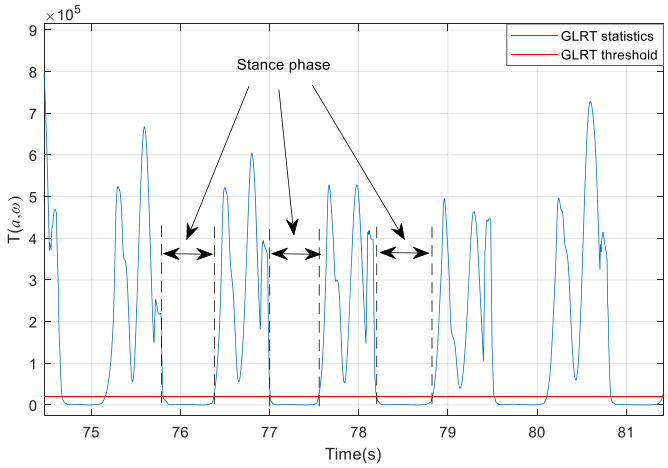

Figure 2. Statistics and threshold of GLRT in gait phase detection.

with the energy in the gyroscope signal, each weighted by the quality of the measurements, falls below th_{GLRT}, the value of $PH_{\mathrm{stance},k}$ is 1, which indicates that IMU-mounted foot is in the stationary period of the step cycle.

Figure 2 shows gait detection by comparing GLRT statistics with the threshold. The GLRT statistics are relatively balanced during the stance period, but the value fluctuates greatly in the swing phase.

3.2. Gait recognition based on height error compensation model

Vertical displacement in SINS is divergent because the influence of gravity cannot be completely removed from motion acceleration. If the height difference at each step obtained by direct integration is taken, misjudgment of the vertical motion may occur. To estimate the vertical motion mode more accurately, the height at each step is first compensated, and then motion classification was performed based on the compensated height.

3.2.1. Error compensation model. Error compensation factor ζ is a key parameter of height compensation model, as shown in formula (5). We build a compensation factor based on an important common sense that the current state of people upstairs and downstairs is related to the last vertical motion state. For example, if a person is currently crossing steps up, the next time he/she is more likely to cross steps up than walk down or horizontally.

$$\zeta = \begin{cases} \frac{\beta}{1+e^{-\|\Delta\tilde{h}\|/h_{\mathrm{str}}}} & \mathrm{cls} > 0 \text{ or } \mathrm{cls} < 0 \\ 0 & \mathrm{cls} = 0 \end{cases} \tag{5}$$

where, $\Delta\tilde{h}$ denotes the height difference based on SINS, cls is the gait state, β is a positive constant, typically set to 0.13. h_{str} represents the height of each stair.

After the error compensation factor is constructed, a height compensation model is proposed, as shown in equation (6). In this model, the movement state (i.e. horizontal movement, downstairs motion, and upstairs motion) of a previous step cycle affects the current height compensation method. If the previous step is horizontal walk, the current height correction is mainly related to the average initial elevation drift. If the previous step is not horizontal, there is a specific proportional relationship between the current height correction and the last height change.

$$\Delta h^{\mathrm{cbl}} = (1 + \zeta \cdot \mathrm{sgn}(\mathrm{cls})) \cdot \Delta\tilde{h} + (1 - \mathrm{sgn}(\zeta)) \cdot \varepsilon \tag{6}$$

where, Δh^{cbl} denotes the corrected height difference for the current step cycle, ζ is error compensation factor, $\Delta\tilde{h}$ is defined as in equation (5), ε indicates the average value of the height error of each step in the initial stage of positioning. sgn(r) is a signum function whose value is 1 when r is greater than 0, -1 when r is less than 0, and 0 when r is equal to 0.

3.2.2. Gait recognition. Generally, gait is divided into three states: walking horizontally, going upstairs and going downstairs. For horizontal walk, the elevation does not change; for going upstairs and downstairs, the number of steps crossed can

be 1, 2, 3, etc. Hence, gait recognition plays an important role in height estimation. The set of gait classification is $\{0, \pm1, \pm2, \ldots, \pm c\}$. The classification result in the ith gait cycle cls_i can be described as:

$$\mathrm{cls}_i = \begin{cases} \mathrm{round}\left(\frac{\Delta h_i^{\mathrm{cbl}}}{h_{\mathrm{str}}}\right) & \|\Delta h_i^{\mathrm{cbl}}\| < \left(c + \frac{1}{2}\right) h_{\mathrm{str}} \\ c \cdot \mathrm{sgn}\left(\Delta h_i^{\mathrm{cbl}}\right) & \text{others} \end{cases} \tag{7}$$

where, c is a constant representing the maximum number of stairs that can be crossed at each step, h_{str} denotes the height of each stair, and round (r) is a function that rounds a real number r to the nearest integer.

3.3. Calculation of prior height

Typically, the stair height of a multi-story building is fixed and easy to get. Assuming that the stair height is h_{str}, there are no changes of height when the pedestrian is in the stationary phase. On the other hand, when the motion states of going upstairs and downstairs are detected, the height difference is related with the motion state and stair height. Thereupon, the updated altitude is calculated as:

$$h_i^{\mathrm{cls}} = h_{i-1}^{\mathrm{cls}} + h_{\mathrm{str}} \cdot \mathrm{cls}_i \tag{8}$$

where, h_i^{cls} and h_{i-1}^{cls} denote the updated altitude based on gait recognition in the ith and $(i-1)$th gait cycles, respectively. The initial value $h_1^{\mathrm{cls}} = 0$.

4. Height calibration with library of floor key points

Generally, the same floor of a building has the same height. This information can be used to eliminate cumulative errors of vertical displacement. To achieve this purpose, it is necessary to first identify whether the user is on a horizontal floor, then establish a floor-height fingerprint database online, and finally, match and calibrate the vertical displacement of users in the floor plane with the floor-height fingerprint database.

4.1. Floor key point detection

Floor key point detection is the first step in correcting elevation using floor information. Different from traditional visual image detection, floor key point detection utilizes inertial data and human behavior characteristics to detect people moving from stairs to floor planes. As shown in figure 3, there are three key quantities to be used for floor key point detection, which are the state of gait transition s_{gtrans}, number of stairs climbed $n_{\mathrm{stair\_clb}}$, and parallel state of flights $\mathrm{parl}_{\mathrm{ft}}$.

The state of gait transition s_{gtrans} refers to the transition from flight to floor plan or to landing.

$$s_{\mathrm{gtrans}} = \begin{cases} 1 & \mathrm{cls}_i = 0, \mathrm{cls}_{i-1} > 0 \\ -1 & \mathrm{cls}_i = 0, \mathrm{cls}_{i-1} < 0 \\ 0 & \text{others} \end{cases} \tag{9}$$

where, cls_i and cls_{i-1} are gait patterns as defined in equation (7).

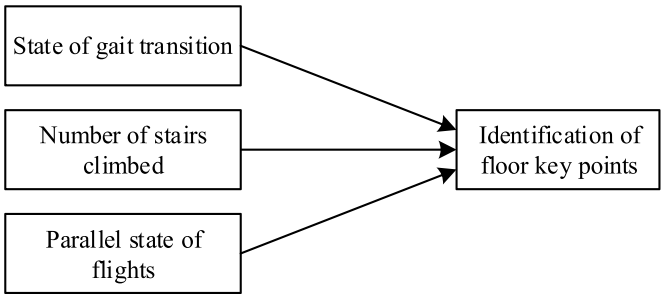

Figure 3. Floor key point detection diagram.

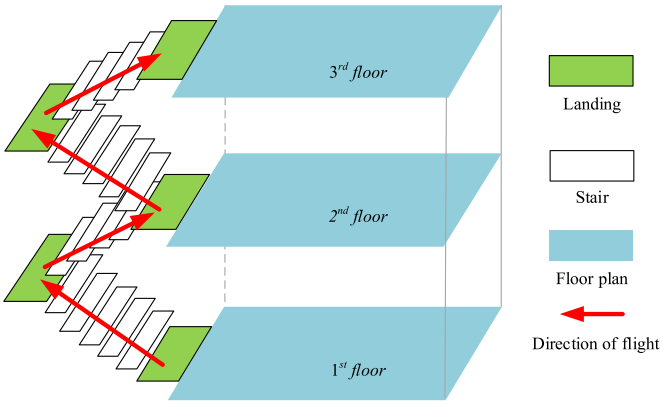

Figure 4. Schematic diagram of building interior structure.

The number of climbing stairs $n_{\mathrm{stair\_clb}}$ involves the number of stairs stepped after leaving the previous floor plan, which is computed as:

$$n_{\mathrm{stair\_clb}} = \sum_{j=1}^{n_{\mathrm{curflr}}} \|\mathrm{cls}_j\| - \sum_{i=1}^{n_{\mathrm{preflr}}} \|\mathrm{cls}_j\| \tag{10}$$

where, n_{curflr} is the total steps at the current moment, n_{preflr} represents the number of stairs climbed when the floor was detected last time.

Flight direction is defined as the direction of the shoe mounted with a sensor. Generally, there are two or three flights between floors as shown in figure 4.

The parallel state between stair flights s_{ftparl} is described as:

$$s_{\mathrm{ftparl}} = \begin{cases} 1 & \mathrm{rem}\left(\|\Delta\psi_{\mathrm{ft}}\|, \mathrm{pi}\right) < \gamma_p \\ & \text{or } \mathrm{pi} - \mathrm{rem}\left(\|\Delta\psi_{\mathrm{ft}}\|, \mathrm{pi}\right) < \gamma_p \\ 0 & \text{others} \end{cases} \tag{11}$$

where, γ_p is the threshold for judging the parallel of flights, $\Delta\psi_{\mathrm{ft}}$ denotes the direction difference between the current flight and the first flight after leaving the previous floor, pi is the circular constant with a value of 3.14, and rem (a, b) is the remainder operation which returns the remainder after division of a and b (a is the dividend and b is divisor).

Based on equations (9)–(11), as well as the threshold γ_{stair} regarding the number of stairs climbed at each floor, the user's floor F on which the user is located will be updated at key

points as follows:

$$F = \begin{cases} F+1 & s_{\text{gtrans}} = 1 \text{ and} s_{\text{ftparl}} = 1 \text{ and } n_{\text{stair}_{\text{clb}}} \geqslant \gamma_{\text{stair}} \\ F-1 & s_{\text{gtrans}} = -1 \text{and} s_{\text{ftparl}} = 1 \text{ and } n_{\text{stair}_{\text{clb}}} \geqslant \gamma_{\text{stair}} \\ F & \text{others} \end{cases} . \tag{12}$$

4.2. Online floor modeling and floor matching

For the existing floor determination approaches, the location fingerprint database needs to be established in advance and the system performance depends on the number of the fingerprint locations. We propose a different method, an online one, for floor-height fingerprint database to correct elevation. Floor-based environment constraints are fundamental for fingerprint database building and matching.

4.2.1. Online floor modeling. The library of floor key points is generated in real time during the positioning process, and does not require external information collection in advance. This library consists of five features {sequence number, floor number, height of each floor, flight direction, and state of gait transition}, which will be developed or updated when equation (12) is satisfied. The constructed database contains a table and follows three rules. First, each row of the table represents the information of floors, and the floor number is unique in the library. Second, when a person arrives at a floor for the first time, the information on that floor needs to be created; otherwise, the information on the existing floor will be updated. Finally, the initial floor should be manually indicated by users.

4.2.2. Floor matching. When pedestrians walk indoors, there are some floor features that can be utilized to limit the height error growth and correct the elevation. For example, at the horizontal level of each floor, when a pedestrian walks on a certain floor of a building or reaches that floor again, his/her altitude remains constant and equals the height of the floor. In addition, the height of each floor is the same except for the ground floor and basement.

If the floor height table of a building is built, floor matching algorithm will be performed as the floor number is updated. We can determine which floor the user is located by comparing the prior height with the constructed table. Floor matching rules as follows:

If

$$\min_{j \in \mathbb{Z}} \sqrt{\left(h_i^{\text{cls}} - h_j^T\right)\left(h_i^{\text{cls}} - h_j^T\right)} < \gamma_{\text{mtch}} . \tag{13}$$

Then

$$j^* = \arg\min \sqrt{\left(h_i^{\text{cls}} - h_j^T\right)\left(h_i^{\text{cls}} - h_j^T\right)} \tag{14}$$

$$h_i^{\text{cls}} = h_{j^*}^T \tag{15}$$

Table 1. Technical specifications of gyroscope and accelerometer in KY-IMU102N-B0.

	Sensor type	
Parameter	Gyroscope	Accelerometer
Bias stability	1.6 °/h	0.03 mg
Bandwidth	200 Hz	200 Hz
Non-linearity	0.02%	0.1%

where, $\mathbb{Z}$ belongs to the set of floor numbers in the floor table, h_i^{cls} is the height calculated according to equation (8), h^T denotes the height in the floor table established online, min is a minimization function, arg min returns the variable value when minimizing the objective function, j^* is the optimal floor number based on floor matching algorithm, and γ_{mtch} represents the threshold for floor matching. Note that height errors could be estimated to provide feedback for EKF.

5. Experiments and analysis

To validate the advantages of the proposed algorithm, this section introduces the equipment, experimental scenario, and experimental results. First, the hardware devices are described, including IMU and embedded processing part. Then, the performance evaluation of the proposed approach is presented and analyzed.

5.1. Data acquisition sensor and test system description

5.1.1. IMU description. The selected IMU module used in IPN should be compact and low-powered with a relatively large measurement range. The KY-IMU102N-B0 IMU module produced by Beijing BDStar Navigation Technology Co., Ltd is chosen as our experimental device. It integrates three orthogonal accelerometers, gyroscopes and magnetometers. Its size is 47 × 44 × 14 mm. The output frequency of the acceleration and angular rate is configured to be 200 Hz, and the operating temperature range of the inertial sensor is −40 to +70 degrees. The related performance parameters are listed in table 1.

5.1.2. Structure of the proposed system. The embedded board mainly contains ultra-low power consumption STM32F4 chip, and Bluetooth communication module (FSC-BT816, FEASYCOM Inc. Shenzhen, China). The hardware structure is shown in figure 5. Raw data is collected and processed by the microcontroller in the embedded board, then the result of height estimation is transmitted to the back-end server through the Bluetooth module.

5.2. Field testing and results

Two experiments were carried out to verify the performance of the proposed algorithm. To solve the problem that the height error of SINS solution would diverge without boundary, gait

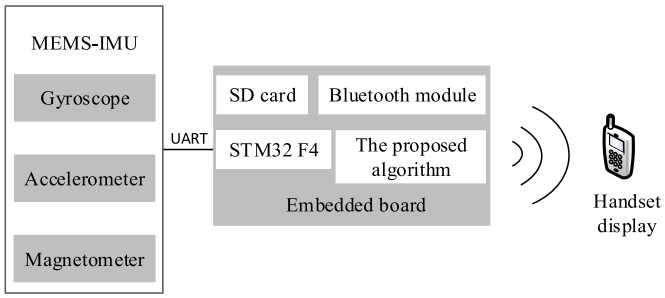

Figure 5. Hardware structure of the proposed system.

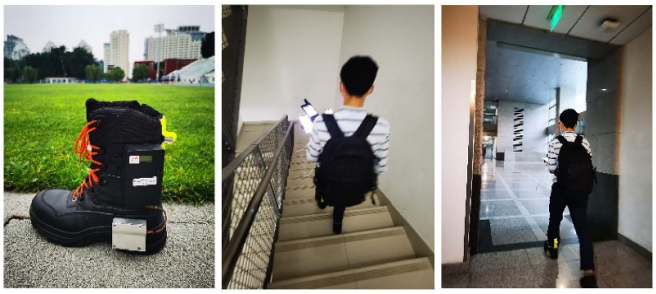

Figure 6. IMU installation and experimental scenario in the building.

recognition based on height error compensation model and floor detection were utilized for height correction. In the experiments related to this paper, the sensor module was mounted on the rear of the left foot, on the lower part of the shoe.

5.2.1. Experiment 1—analysis and results. The first experiment was conducted in Block G, the new main building of Beihang University in Beijing, which is mainly used for teaching and scientific research. Figure 6 presents the experiment scenario in this building.

The building has eleven floors, and the whole altitude difference from the ground floor to top floor is about 43 m. The ground floor has three segment stairs connected by two platforms, and the other floors contain two flights of stairs connected by a platform. In addition, there are 33 stairs on the ground floor, and 26 stairs on the remaining floors, each of which is 16 cm in height. At the beginning of the experiment, the user moved a short distance along the corridor from the origin (0, 0, 0), walked up from the 2nd floor to the 10th floor, then went down to the ground floor, and finally returned to the starting point. The 3D walking route is shown in figure 7: the tester starts from the blue square, moves in the direction of the red arrow, and finally returns to the magenta lower triangle. In the process of going upstairs and downstairs, the tester may cross 1–4 stairs in each step cycle.

In general, a pedestrian does not change his/her vertical displacement during walking on a horizontal plane, but change only for going up and down stairs. We also assume that the altitude at the starting point is 0 m. Figure 8 shows the altitude estimated by barometer, fixed threshold method, the laser

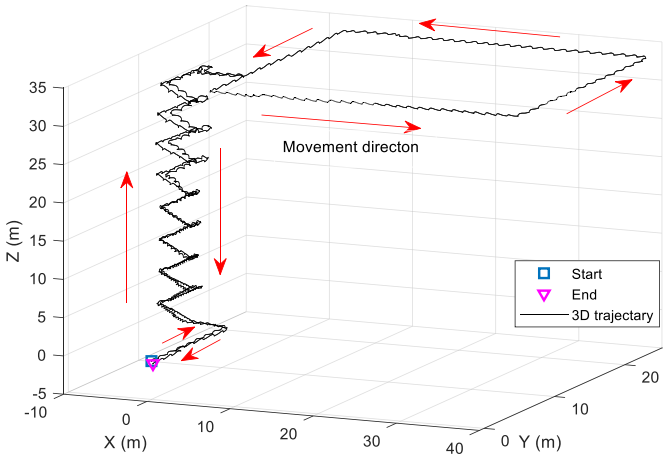

Figure 7. Three-dimensional trajectory map of pedestrians in Experiment 1. The *X*-axis and the *Y*-axis are eastward and northward directions, respectively. The *Z*-axis represents the height relative to the starting point.

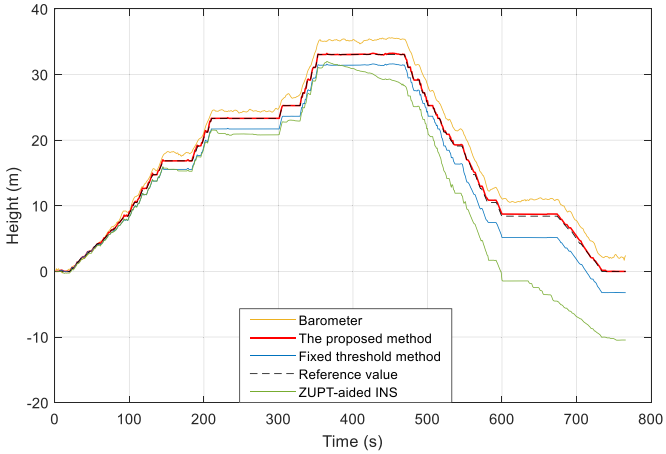

Figure 8. Comparison of altitude estimation algorithms with different heights at each step.

rangefinder, ZUPT-aided INS and the proposed method in the first experiment. The reference height is derived from the interpolation method after the key point height is measured by a laser rangefinder, which is indicated by the black dashed line. The laser rangefinder has millimeter-level positioning accuracy and is suitable for measuring actual vertical trajectory. The yellow line stands for the height track based on the barometer, which are smoothed by the moving average method at a window size of five second. The model of the barometer is SPL06-001 (Goertek, China). During the positioning test, the maximum single point error exceeds 3 m and root mean square (RMS) is nearly 1.7 m, caused by environmental factors including airflow and temperature variations. Compared with the reference value, the green line has obvious fluctuations and is estimated by ZUPT-aided INS. Due to the altitude channel divergence, the maximum single point error and RMS of ZUPT-aided INS are about 10.5 and 6.03 m respectively. To suppress the altitude channel divergence of SINS, gait

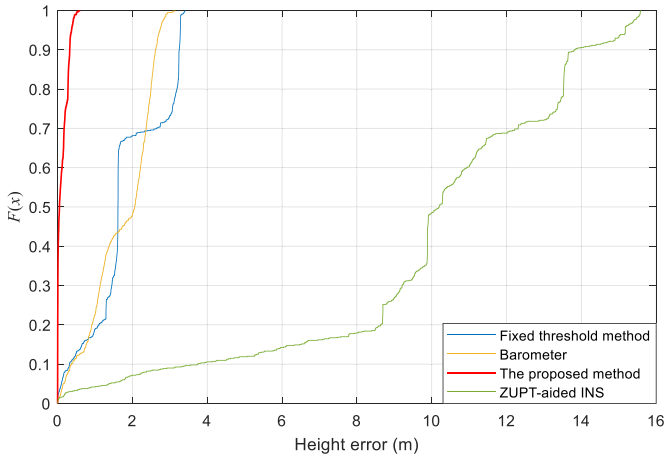

Figure 9. CDF of pedestrian altitude errors.

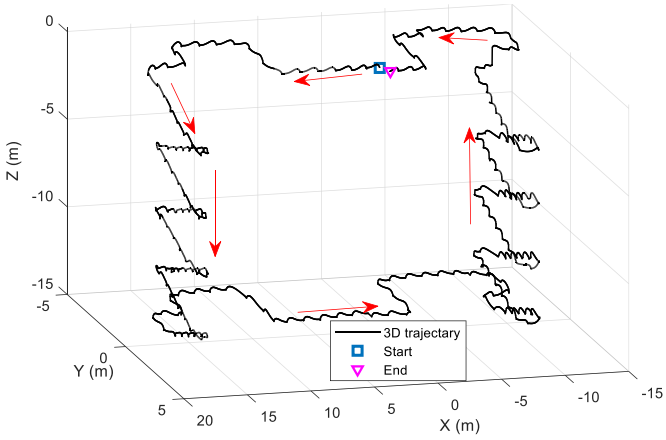

Figure 10. Three-dimensional trajectory map of pedestrians in Experiment 2. The X-axis and the Y-axis are eastward and northward directions, respectively. The Z-axis represents the height relative to the starting point.

recognition is used for height estimation of pedestrians in some documents and height error growth is updated in every stance phase. The blue curve represents height estimation derived from the gait classification based on fixed threshold method. The maximum single point error and RMS of this method are approximately 3.5 and 1.8 m, which are close to the barometric height measurement. To further overcome the limitations of classification effect and error accumulation, both the error compensation model and the floor constraint work to limit the height error growth. Elevation information estimated by the proposed method is indicated by the red line, which is close to the true track shown by the black line. The proposed method is less affected by the environment and performs best with the maximum single point error of 0.74 m and RMS of 0.12 m.

Figure 9 illustrates the cumulative distribution function (CDF) of the altitude errors by using the fixed threshold-based method, the barometer, ZUPT-aided INS, and the proposed method, which are represented by the blue, black, yellow, and red curves, respectively. The abscissa represents the pedestrian altitude errors, and $F(x)$ is defined as the proportion of X values less than or equal to x.

The yellow curve has a large error distribution from 0 to 15.8 m. The main reason for this result is the altitude channel divergent of INS aided by ZUPT. To limit the height error growth, gait recognition based on the fixed threshold method is adopted. As shown by the blue curve, the elevation error range is 0–3.5 m, and the errors less than 2 m account for almost 70%. The black curve denotes the height base on barometric method and the error ratio above 2.3 m is 30%, which is close to that of ZUPT-aided INS method. However, both methods have problems. Barometer-based method is susceptible to environmental impact, and the cumulative error suppression of ZUPT-aided INS needs to be further improved. The proposed method, however, enhances the positioning accuracy by constructing error compensation model and floor constraint. The red curve indicates a relatively concentrated error, ranging from 0 to 0.73 m. These results show the effectiveness of the proposed method in height estimation.

5.2.2. Experiment 2—analysis and results. The second experiment was conducted in Baiyan Building, an office building. The height of the ground floor is 5.1 m, the second and third floors are 4.5 m high, and the remaining floors are 3.6 m in height. The ground floor has four segment stairs connected by three platforms, and the other floors contain two flights of stairs connected by a platform. Furthermore, each stair is 16 cm high.

At the beginning of Experiment 2, the tester moved a short distance along the corridor on the 9th floor from the origin (0, 0, 0), went down to the 5th floor, then walked across the corridor to the staircase on the other side and went up to the 9th floor, and finally returned to the starting point. As shown in figure 10, the tester starts from the blue square, moves in the direction of the red arrow, and finally returns to the magenta lower triangle.

To train and validate SVM and ANN models, we collected foot-mounted inertial data from five individuals with three separate walking trials (horizontal movement, downstairs motion, and upstairs motion).

Figure 11 illustrates the confusion matrices of motion modes based on SVM, ANN, and the proposed method. The total number of steps is 193, with 48 for both upstairs and downstairs and 97 for horizontal walking. In each confusion matrix plot, rows correspond to the predicted class (prediction motion) and columns the true class (true motion). Diagonal green cells correspond to observations correctly classified. Conversely, off-diagonal magenta cells correspond to incorrectly classified observations. When the tester goes upstairs, the proposed method has a minimum number of two misidentifications. In comparison with the method of this paper, SVM generates six misclassifications because the classification results of SVM are susceptible to high noise levels. When the tester walks downstairs and on the ground, all of the three methods correctly recognize the gait, except that ANN misrecognizes the level walking. ANN requires a large amount of data to perform better than other techniques. The row at the

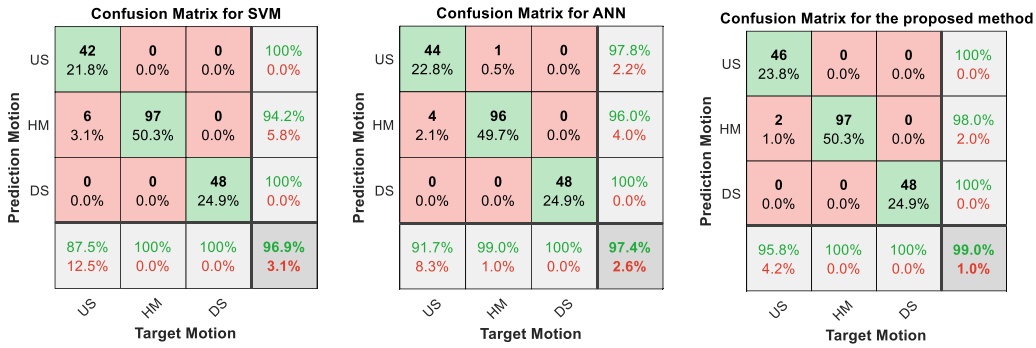

Figure 11. Confusion matrices for motion recognition based on SVM, ANN, and the proposed method. The labels US, HW, and DS indicate upstairs movement, level walking, and downstairs movement, respectively.

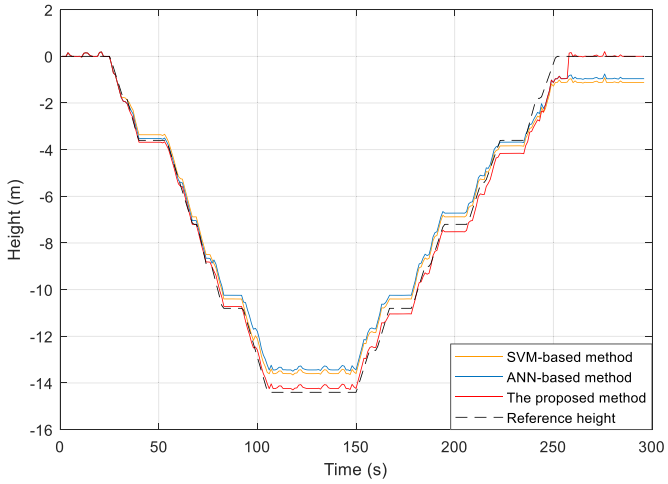

Figure 12. Comparison of heights based on different classification methods for walking upstairs and downstairs.

Figure 13. The testing scenario at the chemical products plant of Sinopec Yanshan petrochemical company.

bottom of the plot shows the percentages of all the examples belonging to each motion mode and correctly and incorrectly identified. The light grey cells are the recall and false negative rate, respectively. For upstairs movement, the recall rate of the proposed method is 95.8%, which is 8.3 and 4.1% higher than that of SVM and ANN, respectively. For downstairs and horizontal walking, the recall rate of SVM and the proposed method has reached 100%. In addition, the element on the bottom right of the plot shows the overall accuracy. The overall accuracy of the proposed method is 99%, 2.1% higher than that of SVM and 1.6% higher than that of ANN. All these results demonstrate the superiority of the proposed approach.

Figure 12 shows vertical displacements achieved by four different methods. The reference height is derived from the interpolation method after the key point height is measured by a laser rangefinder, indicated by the black dashed line. The blue curve and the yellow curve represent the altitude measured by ANN-based method and SVM-based method, respectively. Their performance depends on the accuracy of gait recognition. When the user walks in a loop, compared with the reference height, the cumulative altitude errors of the blue curve and the yellow curve are approximately 1.2 and 1.3 m, respectively. More importantly, the cumulative error will gradually increase. The altitude calculated with the proposed method is represented by the red curve. Due to the contribution of the error model to classification accuracy, the estimated results based on the proposed method are close to the reference height. Additionally, an online floor-height fingerprint database is constructed during walking. Even with a 0.9 m elevation error when returning to the starting floor in a closed-loop walk, the constraints of the floor model effectively eliminate cumulative errors.

5.2.3 Experiment 3—analysis and results. The third experiment was conducted at the Chemical Products Plant of Sinopec Yanshan Petrochemical Company. As depicted in figure 13, the plant environment is complex, featuring metal pipelines and machinery. We simulated a walking trajectory of an inspection personnel and performed repeated tests along this inspection route. The height of the first level in this area is 4.7 m, while the second level is 9.5 m. The ground floor consists of two stair segments connected by a platform, whereas the second floor has only one stair segment without a connecting platform. Additionally, each stair has a height of 0.2 m.

At the beginning of Experiment 3, the tester moved from the origin (0, 0, 0), ascended to the 2nd and 3rd floors, walked across the petrochemical plant area, and finally returned to the starting point. The 3D walking route is depicted in figure 14: the tester starts from the blue square, follows the direction

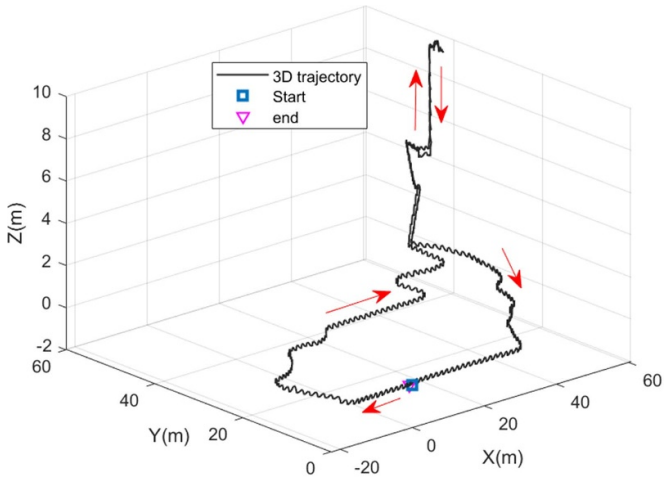

Figure 14. 3D trajectory map of pedestrians in Experiment 3. The *X*-axis represents the eastward direction, the *Y*-axis represents the northward direction, and the *Z*-axis indicates the height relative to the starting point.

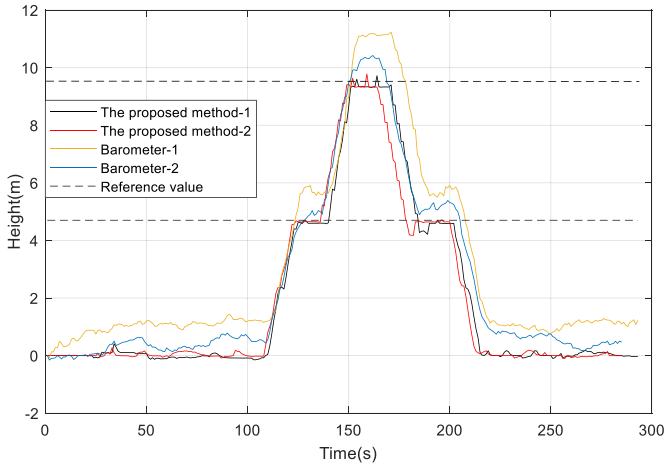

Figure 15. Comparison of altitude in repeated test experiments.

indicated by the red arrow, and eventually returns to the magenta lower triangle.

Figure 15 shows a comparison between the proposed method and barometer-estimated altitudes for two sets of similar trajectories. The reference heights are indicated by two black dashed lines. The blue and yellow curves represent the altitudes measured by the barometer, with maximum errors of 1.1 m and 1.8 m, respectively. These measurements are influenced by factors such as the temperature of the plant equipment and wind speed. The altitudes calculated using the proposed method are shown by the red and black curves, which are generally close. An online floor-height fingerprint database is established during walking. Even with an error of approximately 0.5 m when returning to the second floor, the floor-matching algorithm leverages the element [1, 2, 4.7, −0.53*pi, 1] to eliminate vertical errors. These results demonstrate the accuracy and stability of the proposed altitude estimation method, which combines inertial compensation and online floor modeling.

6. Conclusion

This paper has proposed an altitude determination approach integrating the error compensation model and the floor constraint for a user walking inside a multi-story building with foot-mounted MEMS-IMU. The advantages of this method are as follows. 1) When the level of noise is high, the classification result based on error compensation model is better than that of the traditional methods, and the overall accuracy of the proposed method can reach up to 99%. 2) The floor matching is proposed, totally eliminating cumulative errors. 3) The proposed algorithm is robust to changes in the environment with atmospheric pressure. 4) The proposed algorithm only requires correlation processing of inertial signals, and pre-installation of equipment or collection of fingerprint information is not required. These advantages indicate the effectiveness of the proposed algorithm in vertical localization.

In our future research, we will address the problem of elevation estimation of pedestrians in the case of elevators and escalators.

Data availability statement

The data cannot be made publicly available upon publication because they are not available in a format that is sufficiently accessible or reusable by other researchers. The data that support the findings of this study are available upon reasonable request from the authors.

Acknowledgments

The authors would like to thank the editors and reviewers for their valuable comments, which significantly improved the quality of the manuscript. This work was supported in part by the National Key Research and Development Program of China under Grant 2022YFB3904604 and in part by the 03 Special and 5G Project of Jiangxi Province under Grant 20224ABC03W03.

ORCID iD

Jiale Wang https://orcid.org/0000-0001-6530-7060

References

[1] An J, Yang L and Lee J 2019 Three-dimensional indoor location estimation using single inertial navigation system with linear regression *Meas. Sci. Technol.* **30** 105101
[2] Wang J, Liu J, Zhang S, Xu B, Luo Y and Jin R 2023 Sky-view images aided NLOS detection and suppression for tightly coupled GNSS/INS system in urban canyon areas *Meas. Sci. Technol.* **35** 025112
[3] Li Z, Zhao L, Qin C and Wang Y 2020 WiFi/PDR integrated navigation with robustly constrained Kalman filter *Meas. Sci. Technol.* **31** 084002

[4] Hou B and Wang Y 2024 Positioning by floors based on WiFi fingerprint *Meas. Sci.Technol.* **35** 045003

[5] Qiao J, Hou J, Gao J and Wu Y 2021 Research on improved localization algorithms RSSI-based in wireless sensor networks *Meas. Sci. Technol.* **32** 125113

[6] Li Z, Zhao L, Wang Y, Yang Z, Liu Z and Wang C 2020 Variance optimization of UWB observation based on map matching for PPP/INS/UWB tightly coupled positioning *Meas. Sci. Technol.* **32** 025007

[7] Yu Y, Yang L and Li H 2019 An adaptive model recognition and construction method for RSSI fingerprint-based localization *Meas. Sci. Technol.* **30** 125106

[8] Li F, Tu R, Han J, Zhang S, Liu M and Lu X 2022 Performance research of real-time kinematic/5G combined positioning model *Meas. Sci. Technol.* **34** 035115

[9] Liu M, Tu R, Li F, Chen Q, Li Q, Chen J, Zhang P and Lu X 2024 GPS + 5G fusion for high-precision time transfer *Meas. Sci. Technol.* **35** 045024

[10] Wang J, Zheng F, Hu Y, Zhang, D and Shi C 2023 Instantaneous sub-meter level precise point positioning of low-cost smartphones *NAVIGATION: J. Inst. Navig.* **70** navi.597

[11] Li B, Harvey B and Gallagher T 2013 Using barometers to determine the height for indoor positioning *IEEE Int. Conf. on Indoor Positioning and Indoor Navigation* pp 1–7

[12] Ju H, Lee M S, Park S Y, Song J W and Park C G 2015 A pedestrian dead-reckoning system that considers the heel-strike and toe-off phases when using a foot-mounted IMU *Meas. Sci. Technol.* **27** 015702

[13] Zhang L, Wu J, Jiang C, Jing P and Liu Y 2021 Learning-based stance-phase detection for a pedestrian dead-reckoning system with dynamic gait speeds *Meas. Sci. Technol.* **32** 105108

[14] Wang J, Liu J, Xu X, Yu Z and Li Z 2022 A single foot-mounted pedestrian navigation algorithm based on the maximum gait displacement constraint in three-dimensional space *Meas. Sci. Technol.* **33** 055113

[15] Brigante C M, Abbate N, Basile A, Faulisi A C and Sessa S 2011 Towards miniaturization of a MEMS-based wearable motion capture system *IEEE Trans. Ind. Electron.* **58** 3234–41

[16] Jiménez A R, Seco F, Prieto J C and Guevara J 2010 Indoor pedestrian navigation using an INS/EKF framework for yaw drift reduction and a foot-mounted IMU *2010 7th Workshop on Positioning Navigation and Communication* pp 135–43

[17] Qi L, Yu Y, Liu Y, Gao C and Feng T 2022 Precise 3D foot-mounted indoor localization system using commercial sensors and map matching approach *Meas. Sci. Technol.* **33** 115117

[18] Skog I, Handel P, Nilsson J O and Rantakokko J 2010 Zero-velocity detection-an algorithm evaluation *IEEE Trans. Biomed. Eng.* **57** 2657–66

[19] Sun W, Ding W, Yan H and Duan S 2018 Zero velocity interval detection based on a continuous hidden Markov model in micro inertial pedestrian navigation *Meas. Sci. Technol.* **29** 065103

[20] Xia M and Shi C 2020 Autonomous pedestrian altitude estimation inside a multi-story building assisted by motion recognition *IEEE Access* **8** 104718–27

[21] Wang J, Shi C, Xia M, Zheng F, Li T, Shan Y, Jing G, Chen W and Hsia T C 2024 Seamless indoor–outdoor foot-mounted inertial pedestrian positioning system enhanced by smartphone PPP/3-D map/barometer *IEEE Int. Things J.* **11** 13051–69

[22] Zheng L, Zhou W, Tang W, Zheng X, Peng A and Zheng H 2016 A 3D indoor positioning system based on low-cost MEMS sensors *Simul. Modell. Pract. Theor.* **65** 45–56

[23] Seco F and Jiménez A 2018 Smartphone-based cooperative indoor localization with RFID technology *Sensors* **18** 266

[24] Li Y, Zhuang Y, Zhang P, Lan H, Niu X and El-Sheimy N 2017 An improved inertial/wifi/ magnetic fusion structure for indoor navigation *Inf. Fusion* **34** 101–19

[25] Hartmann F, Rifat D and Stork W 2016 Hybrid indoor pedestrian navigation combining an INS and a spatial non-uniform UWB-network improving *Proc. 19th International Conf. Information Fusion* (*Heidelberg, Germany*) pp 549–56

[26] Qiu S, Wang Z, Zhao H and Hu H 2016 Using distributed wearable sensors to measure and evaluate human lower limb motions *IEEE Trans. Instrum. Meas.* **65** 939–50

[27] Puyol M, Bobkov D, Robertson P and Jost T 2014 Pedestrian simultaneous localization and mapping in multistory buildings using inertial sensors *IEEE Trans. Intell. Transp. Syst.* **15** 1714–27

[28] Laoudias C, Moreira A, Kim S, Lee S, Wirola L and Fischione C 2018 A survey of enabling technologies for network localization, tracking, and navigation *IEEE Commun. Surv. Tutorials* **20** 3607–44

[29] Abdulrahim K, Hide C, Moore T and Hill C 2012 Using constraints for shoe mounted indoor pedestrian navigation *J. Navig.* **65** 15–28

[30] Diaz E, Kaiser S and Ahmed D 2018 Height error correction for shoe-mounted inertial sensors exploiting foot dynamics *Sensors* **18** 888

[31] Yao Y and Luo X-L 2020 Improving vertical positioning accuracy with the weighted multinomial logistic regression classifier *SN Appl. Sci.* **2** 1445

[32] Wagstaff B, Peretroukhin V and Kelly J 2017 Improving foot-mounted inertial navigation through real-time motion classification *2017 Int. Conf. on Indoor Positioning and Indoor Navigation (IPIN)* pp 1–8

[33] Grzonka S, Karwath A, Dijoux F and Burgard W 2012 Activity-based estimation of human trajectories *IEEE Trans. Robot.* **28** 234–45

[34] Deng Z, Wang P, Yan D and Shang K 2020 Foot-mounted pedestrian navigation method based on gait classification for three-dimensional positioning *IEEE Sens. J.* **20** 2045–55

[35] Ye H *et al* 2012 FTrack: infrastructure-free floor localization via mobile phone sensing *IEEE Int. Conf. on Pervasive Computing and Communications* pp 2–10

[36] Elhoushi M, Georgy J, Noureldin A and Korenberg M J 2016 Motion mode recognition for indoor pedestrian navigation using portable devices *IEEE Trans. Instrum. Meas.* **65** 208–21

[37] Roh S-B, Ahn T-C and Pedrycz W 2010 The refinement of models with the aid of the fuzzy-nearest neighbors approach *IEEE Trans. Instrum. Meas.* **59** 604–15

[38] Guinness R E 2015 Beyond where to how: a machine learning approach for sensing mobility contexts using smartphone sensors *Sensors* **15** 9962–85

[39] Wang J *et al* 2024 Multi-frequency smartphone positioning performance evaluation: insights into A-GNSS PPP-B2b services and beyond *Satell. Navig.* **5** 25

[40] Lu J *et al* 2018 Hybrid navigation method of INS/PDR based on action recognition *IEEE Sens. J.* **18** 8541–8

[41] Bebek O *et al* 2010 Personal navigation via shoe mounted inertial measurement units *2010 IEEE/RSJ Int. Conf. on Intelligent Robots and Systems* pp 1052–8